Fifth International Conference on CFD in the Process Industries
CSIRO, Melbourne, Australia
13-15 December 2006

FLOW AND PARTICLE DEPOSITION PATTERNS IN A REALISTIC HUMAN DOUBLE BIFURCATION AIRWAY MODEL

Lok-Tin CHOI and Jiyuan TU

School of Aerospace, Mechanical and Manufacturing Engineering,
RMIT University, PO Box 71, Plenty Road, Bundoora, Victoria 3083, AUSTRALIA

ABSTRACT

Velocity profiles, local deposition efficiencies (DE) and deposition patterns of aerosol particles in the first three generations (i.e. double bifurcations) of an airway model have been simulated numerically, in which the airway model was constructed from CT scan data of real human tracheobronchial airways. Three steady inhalation conditions and a range of micron-particle sizes were simulated. The results indicate that the local DE in the first bifurcation increase with a rise in the Stokes number (St). DE in the second bifurcations (both left and right) is dropped dramatically after St increased to 0.17. Also, the second bifurcation in the right side was found to show a much higher (almost double) DE than the left side. This may be due to the fact that the left main bronchus is longer and has greater angulation than the right main bronchus. The present simulation proved that the current technique developed would be useful in clinical study.

Keywords: tracheobronchial airways; CT scan, Aerosol transport and deposition; Computational two-phase flow

NOMENCLATURE

A	cross-sectional inlet area
C_D	drag coefficient
D	Diameter
dp	particle diameter
F_D	drag force
k	turbulence kinetic energy
L	Length
Le	eddy length scale
p	pressure
Q	Respiratory rate of inhalation
r	uniform random number
Re	Reynolds number
Re_p	particle Reynolds number
St	Stoke number
t	time
t_{cross}	particle eddy crossing time
t_p	particle relaxation time
T_L	Lagrangian integral time
u	velocity
u_i	velocity vector (same for u_j)
μ	dynamic viscosity
u^g	gas (air) velocity
u^p	particle velocity
U	mean velocity
x_i, x_j, x_k	spatial coordinate system

Greek letters

ρ	density
ω	Pseudo-vorticity
v	kinetic viscosity
τ_e	eddy lifetime
τ_i	Reynolds stress tensor

Subscripts and Superscripts

air	air phase
p	particle phase
g	gas phase
k	turbulent kinetic energy
p	discrete particle phase
t	turbulent phase

INTRODUCTION

Inhaled particle pollutants have been implicated as a potential cause of respiratory diseases. Therefore, accurate prediction of local and regional pattern of inhaled particle deposition in the human airway should provide useful information to clinical researchers in assessing the pathogenic potential and possibly lead to innovation in inhalation therapies.

There are two major types of airway geometry models used in assessing the velocity profile and deposition efficiency (DE) in an experiment: human airway casts from cadavers (Schlesinger, Gurman & Lippmann, 1982) and idealized geometries, constructed by series of smooth-walled tube with (Kim & Fisher, 1999) or without regular dichotomy (Chang & El Masry, 1982). In numerical studies, a smooth-walled (and hence simplified) airway model was mostly employed with only variation in geometry and method of dichotomy. Regular dichotomy (symmetry) airway models have been extensively studied by Zhang, Kleinstreuer, & Kim (2002). All these studies show that the regional deposition efficiency (DE) can be expressed as a logistic function in terms of inlet Stokes (St) number for any bifurcation geometry. Moreover, both experimental and numerical studies indicated that the variation of the logistic function is basically dependent on geometrical factors of the model.

Schlesinger, Gurman and Lippmann (1982) measured the particle deposition for the first five branching generations of replicate hollow casts of a human tracheobronchial tree. Kim and Fisher (1999) established a logistic function to describe the DE that they measured on a double bifurcation model with dimensions similar to G3-G5 in Weibel's (1963) symmetrical model. Their results showed that DE in each bifurcation increased with increasing Stokes number. Chang & El Masry (1982) illustrated detailed steady inspiratory velocity profiles in a scaled model of the human central airways, in which the model geometry was similar to the present CFD model. Zhang & Finlay (2005) proved that trachea with cartilaginous rings would enhance particle deposition in the trachea for all inhalation rates and particle sizes when compared with smooth-walled trachea.

Although, particle deposition and its dynamic nature have been investigated comprehensively by experimental

studies on casts of human airways and the simplified (smooth-walled) model as well as numerical studies on simplified models in different geometrical configurations, it is still unclear to what extent the results from these studies may be applied to numerical predictions based on a model of realistic human tracheobronchial airway that was replicated using CT scan data. It is because geometrical details of human airway are not identical among people and these may strongly affect the prediction on both the airflow and the regional particle deposition. Therefore, this study was conducted to evaluate the potential use of CFD in assisting practical clinical study. An airway model was constructed from CT scan data and the suitability and comparability of the CFD model will be determined by comparing the air flow and particle deposition efficiency with other data.

METHODS

Geometry generation and field equations: Airway geometry was obtained through a computed tomography (CT) scan of the airways of a healthy 25 year old, non-smoking Asian male (170 cm height, 75 kg mass) for the first three generations. With the given CT scan data of human tracheobronchial airways consisting of the trachea and the main bronchi, a CFD model was reconstructed. Figure 1 illustrated how the measurement of the dimension of the airways was conducted and how the bifurcation and generation were segmented in the airways. The model was constructed using GAMBIT. A mesh independent test was conducted using 0.05, 0.45, 1.6 and 2.1 million tetrahedral cells. By comparing the velocity profiles and DE, 0.45 million cells was found to be suitable in terms of computational time and accuracy. The approximate geometric measurements of the model are provided in Table 1. Small modifications were made to the model to round sharp curves and to extended bronchus (as shown in Figure 1) in order to avoid back-flow phenomena that may affect the convergence process.

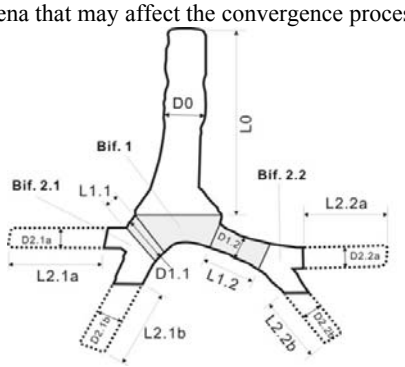

Figure 1: Realistic double bifurcation airway model segmentation (bifurcations and generations, the shaded region indicates the first bifurcation and the dashed line indicates the extended tubes for CFD purpose)

The parameters of the inlet flow and associated particle characteristics are summarized in Table 2. There are three practical reasons for choosing these parameters: firstly, most of the experimental and numerical data available have been obtained under these particular inlet flow rates; secondly, the flow rates are typical of what a human would experience during different exercise conditions; thirdly, the chosen particle size range is typical of those particles from inhalers that can reach the first few generations of airways (consisting of the trachea and the main bronchi (Edward, 2002)).

Generation	0 (Trachea)	1	2
Diameter	D0 1.54	D1.1 1.65 D1.2 1.02	D2.1a 0.99 D2.1b 1.1 D2.2a 0.83 D2.2b 0.84
Length	L0 9.26	L1.1 0.73 L1.2 1.79	L2.1a 4.55 L2.1b 3.11 L2.2a 3.75 L2.2b 2.57

Table 1. Morphometry of the tracheobronchial tree model (Dimensions in centimetre)

Physical state	Resting	Light activity	Moderate exercise
Respiratory rate of inhalation (Q, L/min)	15	30	60
[a]Mean Reynolds number at inlet	1447	2894	5789
Particle diameter (d_p, μm)	1 − 20		
Particle density (ρ_p, kg/m3)	1550		
[b]Mean Stokes number at inlet	0.00042 − 0.17	0.0008 − 0.33	0.002 − 0.66

[a] Reynolds number, $\mathrm{Re} = UD\rho_{air}/\mu$
where U is evaluated as Q/A

[b] Stokes number, $St = \rho_p d_p^2 U/(18\mu D)$

Table 2. Representative respiration data and particle parameters

According to Wilcox (1998), the low Reynolds number (LRN) k-ω model should be used in capturing the air flow structures in the laminar to turbulent flow regimes for internal flow (Zhang and Finlay, 2005). FLUENT 6.1.22 was used to solve the following incompressible fluid flow equations. The model solved is entirely built in to FLUENT without any external code (User-Defined-Function) used.

Continuity equation

$$\frac{\partial \overline{u}_i}{\partial x_i} = 0 \quad (1)$$

Momentum equation

$$\overline{u}_j \frac{\partial \overline{u}_i}{\partial x_j} = -\frac{1}{\rho}\frac{\partial p}{\partial x_i} + \frac{\partial}{\partial x_j}\left[(\nu + \nu_T)\left(\frac{\partial \overline{u}_i}{\partial x_j} + \frac{\partial \overline{u}_j}{\partial x_i}\right)\right] \quad (2)$$

Turbulence kinetic energy (k) equation

$$\overline{u}_j \frac{\partial k}{\partial x_j} = \tau_{ij}\frac{\partial \overline{u}_i}{\partial x_j} - \beta^* k\omega + \frac{\partial}{\partial x_j}\left[(\nu + \sigma_k \nu_T)\frac{\partial k}{\partial x_j}\right] \quad (3)$$

Pseudo-vorticity (ω) equation

$$\overline{u}_j \frac{\partial \omega}{\partial x_j} = \alpha\frac{\omega}{k}\tau_{ij}\frac{\partial \overline{u}_i}{\partial x_j} - \beta\omega^2 + \frac{\partial}{\partial x_j}\left[(\nu + \sigma_\omega \nu_T)\frac{\partial \omega}{\partial x_j}\right] \quad (4)$$

For convenience, summation notation is used with *i, j =1,2,3*. v_T is given as $v_T = C_\mu f_\mu k/\omega$, and the function f_μ is defined as $f_\mu = exp[-3.4/(1+R_T/50)^2]$ with $R_T = k/(\mu\omega)$ and μ being the dynamic molecular viscosity ($\mu = \rho\nu$). C_μ, α, β, β^*, σ_k, and σ_ω are turbulence constant, i.e. (Wilcox,

1998): C_μ = 0.09, α = 0.555, β = 0.8333, β^* = 1 and σ_k = σ_ω = 0.5.

For a low volume fraction of dispersed particle phase, an Eulerian-Lagrangian approach has been used. One-way coupling between air and particle phases was assumed. Also, the interaction between particles is neglected to reduce computational cost.

Trajectories of individual particles can be tracked by integrating the force balance equations on the particle. Equation (5) did not include other possible forces that a particle may experience during a real experiment. These forces were neglected in order to simplify the current study and hence formulate the results to be suitable for broaden range of comparison; firstly, gravitational force is being neglected because only inertia cause of deposition is being focused in this study. Secondly, the Brownian force can be neglected, since these effects should only be included for sub-micron particles only. Thirdly, the particulate material considered is far denser than air, causing terms that depend on the density ratio, such as the pressure force, buoyancy force, virtual mass effect and Basset force to be very small. Finally, the Saffman's lift force cannot be included due to relatively large particles and low-level fluid shear fields. The simplified particle trajectory equation (i.e., Equation (5)) was solved numerically using stochastic tracking model and random-Eddy-lifetime (random walk) model. The injected particles were specified to be a smooth and spherical object.

Particle trajectory equation

$$\frac{du_i^p}{dt} = F_D\left(u_i^g - u_i^p\right) \quad (5)$$

The drag force per unit particle mass is $F_D\left(u_i^g - u_i^p\right)$and F_D is given by

$$F_D = \frac{18\rho}{\rho_p d_p^2}\frac{C_D \,\mathrm{Re}}{24} \quad (6)$$

Re is the particle Reynolds number, which is defined as

$$\mathrm{Re} \equiv \frac{\rho d_p \left|u^p - u^g\right|}{\mu} \quad (7)$$

The drag coefficient, C_D, is evaluated from an experimental-fitted expression

$$C_D = a_1 + \frac{a_2}{\mathrm{Re}_p} + \frac{a_3}{\mathrm{Re}_p} \quad (8)$$

where a_1, a_2, and a_3 are constants that apply for smooth spherical particles over several ranges of Re_p given by Morsi and Alexander (1972).

In the stochastic tracking method, FLUENT predicts the turbulent dispersion of particles by integrating the trajectory equations for individual particles, using the instantaneous fluid velocity, $u_i^g + u_i'(t)$ along the particle path during the integration process. With this method, discrete random walk or "eddy lifetime" model, is applied where the fluctuating velocity components, u_i' that prevail during the lifetime of the turbulent eddy are sampled by assuming that they obey a Gaussian probability distribution, so that

$$u_i' = \xi\sqrt{\overline{u_i'^2}} \quad (9)$$

where ξ is a normally distributed random number, and the remaining right-hand side is the local root mean square (RMS) velocity fluctuations that can be obtained (assuming isotropy) by

$$\sqrt{\overline{u_i'^2}} = \sqrt{2k/3} \quad (10)$$

The interaction time between the particles and eddies is the smaller of the eddy lifetime, τ_e and the particle eddy crossing time, t_{cross}. The characteristic lifetime of the eddy is defined as

$$\tau_e = -T_L \log(r) \quad (11)$$

where $T_L \approx 0.15/\omega$. The variable r is a uniform random number between 0 and 1. The particle eddy crossing time is given by

$$t_{cross} = -t_p \ln\left[1 - \left(\frac{Le}{t_p\left|u_i^g - u_i^p\right|}\right)\right] \quad (12)$$

where $t_p = \rho_s d_p^2 / 18\rho_g v_g$ and $\left|u_i^g - u_i^p\right|$ is the magnitude of the relative velocity. The particle interacts with the fluid eddy over the interaction time. When the eddy lifetime is reached, a new value of the instantaneous velocity is obtained by applying a new value of ξ in Equation (9).

Boundary conditions

The airway walls were set as trap in particle boundary condition based on the assumption that the wall of the airway is usually wet, and so once a particle hits the wall it would be trapped.

The final number of particles and the particle flow rate were determined by increasing the number of particles inhaled and decreasing the flow rate until the deposition efficiency became statistically independent of the total number of particles, in which the number of particle to be injected was determined to be approximately 180,000 during one constant inhalation. The DE is defined as the ratio of the number of particles deposited in a given region to the total number entering the region. Due to the low volume fraction of particles over fluid, one-way coupling between these two phases was assumed; i.e., the flow influences the paths of the particles, but the particles do not affect the flow (Crowe et al., 1996).

RESULTS & DISCUSSION

Model Validation

The DE of aerosol particle in double bifurcation airway model for different flow rates and particle sizes (i.e. Stokes number) has been validated with various experimental data sets (cf. Kim & Fisher, 1999; Schlesinger, Gurman, & Lippmann, 1982). Kim & Fisher (1999) suggested modified logistic functions to describe DE vs. Stokes number for the first two bifurcations, which were based on the trend lines fitted on experimental data. Schlesinger, Gurman, & Lippmann (1982) measured the DE on the replicate hollow casts from a solid cast of a human tracheobronchial tree for the first five branching generations. Figure 2 shows the experimental data and CFD predicted deposition efficiencies for the first two bifurcations in range of St 0.01 to 0.12. When comparing the experimental results between a replicate human cast model and a symmetrical glass tube model, there is small differences in DE when the Stokes number is less than 0.1. Similarly, when comparing DE between CFD prediction and experimental data, the differences are approximately within 5% in DE term.

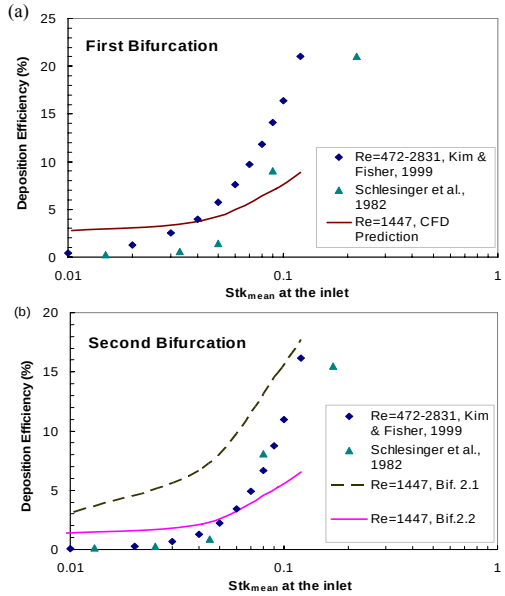

Figure 2(a): Comparison of the predicted and experimental particle deposition efficiency (DE) at (a) first bifurcation and (b) second bifurcation.

Due to the difficulty in precisely controlling the experimental conditions, such as flow rate and aerosol size, the Reynolds number and Stokes number fluctuated in a measurable range. In addition, the differences between experimental measurements and computational predictions can be caused by discrepancies in model geometries (e.g. branching angle of bifurcation, bronchial length). Since the model was constructed based on a realistic airway, the model is unique in terms of geometrical details. Therefore, it is not practical to divide the bifurcation zones and generations based on other results that were mentioned previously. However, the general configuration in dividing the bifurcation zones were carefully compared with other researcher's work (e.g. Zhang, Kleinstreuer & Kim, 2002 and Chang & El Masry, 1982) in order to achieve comparable results. Therefore, when the experimental uncertainties and differences in geometry were considered, the characteristics of the CFD results reasonably correspond to the experimental data.

Axial velocity profiles

Figure 3 (a) and (b) show two sets of normalised axial velocity profiles in the trachea at two flow rates (15 and 60 l/min) in order to investigate the development of particle deposition within airways. The results were validated with Chang and El Masry's (1982) experimental data (plotted as square dots). The numerical results generally have good agreement with experimental results in terms of characteristic features. The small differences in some of the stations are to be expected since the experimental model was made of smooth plastic tubes and the flow rates used in experiment and numerical simulation were different.

Figure 3(a) and (b) show that both entering profiles were of a parabolic shape, although they were beginning to develop into a different profile shape, due to the different flow rate. Figure 3(a) shows that the profiles from station T2 were flatter than the profiles in Figure 3(b). Also, the profiles started to develop into a bi-peak structure from station T5 to T6. Comparatively, the profiles in Figure 3(b) were more parabolic in shape. Both velocity profiles at T5 had a low velocity zone near either one or both ends but both profiles at T6 show that the fluid recovered its inertia force. This phenomenon indicates that there were flow separations between T5 and T6 near the outer wall due to a sudden change in diameter. However, the higher velocity profiles at T4 to T6 also show that, due to greater inertial force, the flow separation seemed to be more sensitive to change in diameter. Therefore, the velocity profiles in the lower flow rate at station T6 was more moderate compared to the higher flow rate, which has peak flow concentrated in the middle of the airway.

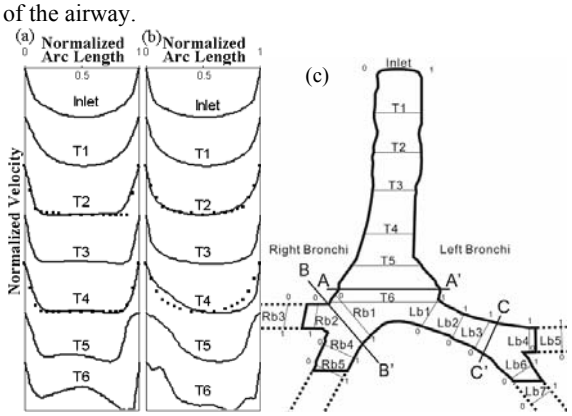

Figure 3: Normalized velocity profile at trachea for an inspiratory flow rate at (a) 15 l/min and (b) 60 l/min, plotted as a function of the normalized arc length. The experimental data of Chang & El Masry (1982) are plotted as (■) for the corresponding stations. Abscissa 0 and 1 correspond to the marks, 0 and 1 in Figure 3(c). (c) View of station position (The letter T represents Trachea; Rb and Lb represent the Right and Left side of Bronchus respectively.)

In Figure 4, the velocity profile in the right bronchus (Rb1) at 15 l/min was more moderate than 60 l/min and it had a high peak near the outer wall (abscissa 0) of the first bifurcation while the profile at 60 l/min was highly skewed toward the inner wall of the first bifurcation. Further downstream in the right upper (Rb2 and Rb3) and lower (Rb4 and Rb5) bronchi, the axial velocity profiles generally continued the basic structure from the previous profiles (Rb1). At lower flow rate, the profiles in the upper bronchi were skewed toward the inner wall of the second bifurcation while the velocity magnitudes were lower near the outer wall (abscissa 0). This phenomenon is likely to be caused by the flow separation or mild reverse flow near the bend of the first bifurcation (near Rb2). However, the higher flow rate was able to overcome the adverse pressure gradient near the outer wall of the first bifurcation due to its greater momentum (as discussed by Chang and El Masry (1982)). On the other hand, due to the greater inertia forces (higher flow rate) from the upstream which caused significant pressure on the carina ridge of the second bifurcation, the velocity near the inner wall was either mild and reversed or very slow, so the velocity profiles were low in the inner wall and high in the outer wall of the second bifurcation.

Three sets of velocity profiles at left bronchus (Lb1 Lb2 and Lb3) are presented in Figure 4. At the lower flow rate, profile at Lb1 was like a mirror image of the profile at the other side (Rb1) where the low velocity zone near the outer wall (abscissa 1) was caused by flow separation. But, the profiles at Lb2 and Lb3 show that the flow

separation was reattached at a short distance from Lb1 due to the low velocity flow. With the higher flow rate, the profile at Lb1 had slow fluid motion near outer wall of the first bifurcation due to large branching angle where again the flow separation or mild reverse flow occurred near the outer wall of bifurcation. But the fluid at Lb2 and Lb3, near the outer wall (abscissa 1) soon accelerated from a low velocity. This phenomenon can be explained by the transverse momentum exchange associated with higher Reynolds number flows as suggested by Chang and El Masry (1982).

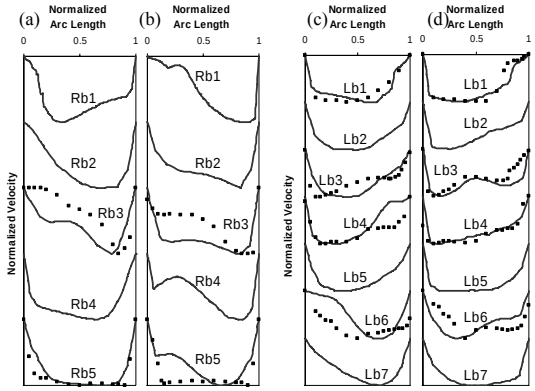

Figure 4: Normalized velocity profile at bronchus for an inspiratory flow rate at (a) & (c) 15 l/min and (b) & (d) 60 l/min, plotted as a function of the normalized arc length. (Refer Fig. 3(c) for station position).

At flow rate of 15 l/min, both the upper (Lb4 and Lb5) and the lower (Lb6 and Lb7) bronchi had peak velocities skewed toward the inner wall of the second bifurcation and a very low velocity near outer wall. This indicated flow separation. In comparison, there was no flow separation observed near the outer wall using the 60 l/min flow rate. Also the peak flow in the upper bronchi (Lb4) skewed toward the inner wall was relatively moderate compare to Lb4 at the 15 l/min flow rate. Surprisingly, the peak flow in the lower bronchi (Lb6) skewed more towards the outer wall of the second bifurcation, which is also the extension from the inner wall of the first bifurcation.

Regional deposition efficiencies

Deposition efficiency (DE) is an important quantitative parameter, defined as the percentage of particles that are trapped on a designated airway surface (such as bifurcation or zone) with respect to the total number of particles entering the respiratory system. As discussed in Model Validation, three bifurcations were divided as shown in Figure 1. Figure 5 summarizes all the DE results collected within this numerical simulation and illustrate them with respect to individual bifurcation in three different inlet flow rates.

The DEs at Stokes number range from 0.0004 – 0.01 in every bifurcation were quite even. The DE at the right second bifurcation (B2.1) increased more considerably than both B1 and B2.2 as soon as Stokes number exceeded 0.01. The second bifurcation in both sides (B2.1 and B2.2) seemed to reach their maximum DE in the tendency of the line when Stokes number reached 0.18 and on the contrary, the DE in the first bifurcation tended to increase even faster after St = 0.18. Nonetheless, the DE in the right second bifurcation (B2.1) was still considerably higher than the left second bifurcation (B2.2). This was also shown by comparing Figure 5b and c with a Stokes number smaller than 0.18. The reason that B2.1 had a higher DE than B2.2 was that the left bronchus (B2.2 side) is considerably longer than right bronchus. This means that particles have to travel further to reach the region of B2.2 which in turn reduces the chance for a particle to be trapped in region B2.2 because part of the particles were trapped along the left bronchus.

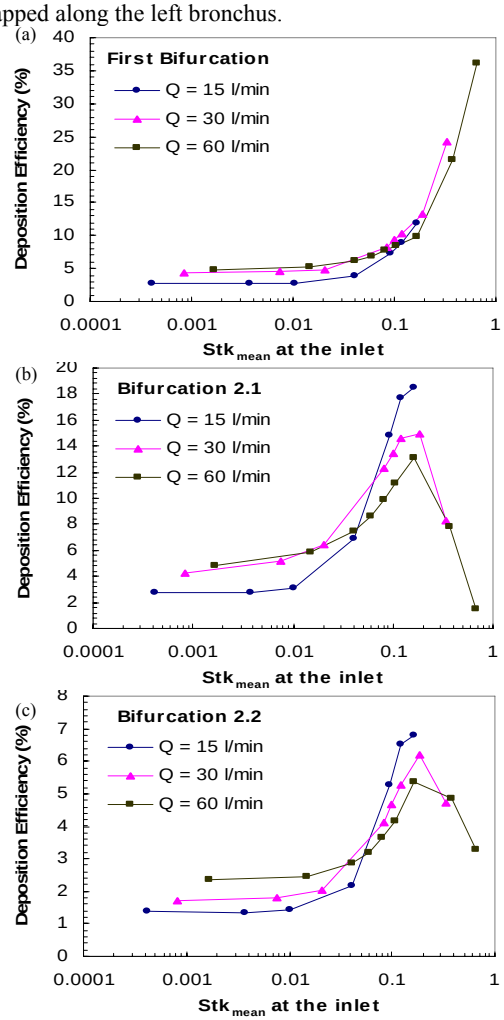

Figure 5: Plot of deposition efficiencies for first bifurcation in the bifurcation airway model against particle diameter and mean Stoke number at the inlet.

Figure 5a shows that a higher Stokes number gave higher DE in the first bifurcation. As expected, the high inertial force created by large particles and/or high flow rate led to a high DE. It should be noted that this only happened in the first bifurcation. In the second bifurcations, the previous characteristic only applied for Stokes number smaller than 0.18. As depicted in Figure 5b and 7c, the DE dropped when the Stokes number rose to 0.18. This was due to the fact that more particles were already trapped in the first bifurcation as Stokes number increased and hence it decreased the number of particles travelling to lower generations. As a result, lower Stokes number was more efficient to transport particles to the second bifurcation. Moreover, Figure 5 proved that the mean Stokes number at the inlet is actually a good index of predicting DE. There are minor DE differences, however there are acceptable when the possible error (discussed in Model Validation) was taken into account.

Particle deposition patterns

Four graphical deposition patterns were depicted on a three-dimensional airway model with four typical conditions using the same model as shown in Figure 6 and 7. Although, the plot of DE against inlet Stokes number already addressed the DE information, the complete view of the deposition pattern can definitely help to investigate how the flow pattern affects the particle deposited into the airway in a more visually assessable form.

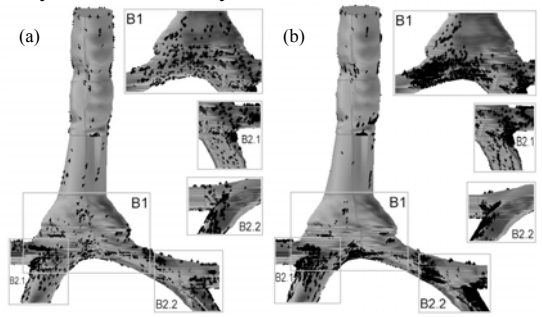

Figure 6: Deposition pattern in 3D views for 15 l/min with particle diameter in (a) 10 μm (St_{mean} = 0.042, Re_{mean} = 1447), (b) 20 μm (St_{mean} = 0.166, Re_{mean} = 1447).

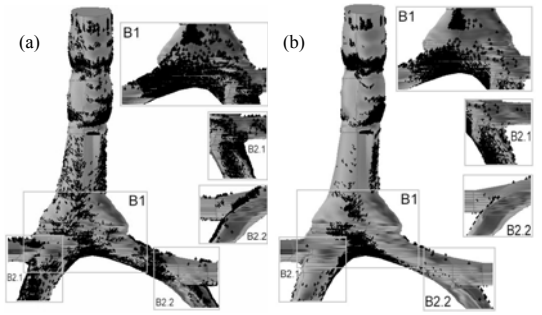

Figure 7: Deposition pattern in 3D views for 60 l/min with particle diameter in (a) 10 μm (St_{mean} = 0.166, Re_{mean} = 5789), (b) 20 μm (St_{mean} = 0.665, Re_{mean} = 5789).

Figure 6b and 7a show that even for the same Stokes number (both at St = 0.166), the deposition patterns were markedly different, especially the pattern along the trachea. This indicates that DE-St number plot is not sufficient to provide details of particle deposition.

The axial velocity profile at station T6 in the trachea (Figure3a) for 15 l/min flow rate demonstrated that the "M" shape velocity profile gave relatively high particle densities in both sides (B2.1 & B2.2) and low densities in the middle (B1) in Figure 6 a and b. Correspondingly, the velocity profile at station Rb1 (Figure 4a) was moderate so that both the outside and the inside wall of second bifurcation (B2.1), as well as the carina ridge, collected noticeable amount of particles. At another side, the velocity profile at station Lb3 skewed slightly toward the bottom bronchus, but still retained a moderate velocity in the middle. As a result, the bottom left bronchus and the carina ridge captured a higher amount of particles (see Box B2.2 in Figure 6b). These phenomena were more obvious in Figure 6b where larger particles were injected with the same flow rate. The difference was that the locations mentioned contained higher particle densities and were less diffuse.

Figure 7a and b show that a high flow rate increased the chance for the region facing directly towards the flow to collect a larger amount of particles. When smaller particles were injected (Figure 7a), a diffusive phenomenon dominated the behaviour of particle transportation. This was why a large amount of particles deposited along the trachea. However, due to the moderate Stokes number, the model also contained high particle densities in all bifurcations and the inner wall leading down from the carina ridge in all bifurcations. On the contrary, when large particles were injected, convective phenomenon became dominated. In addition, particle densities were more intensive and concentrated into the first bifurcation and the inner wall leading down from the carina ridge in the first bifurcation as shown in Figure 7b.

CONCLUSION

The validated CFD analysis of the realistic double bifurcation airway model proves that the present CFD model can provide reasonable results. In terms of the deposition pattern, the cartilaginous rings in the trachea can have a major influence on DE in the trachea. This is especially obvious when the flow rate is large. Also, high particle densities were observed along carina ridge and the inner wall leading down from the carina ridge in all bifurcations. However with various Stokes numbers, particle density can be concentrated in either (or both) inner wall. Although, the local DE can be predicted by using Stokes number, conditions with the same Stokes number are not necessarily the same in terms of local deposition pattern and particle density. Further studies are needed to extend the results to other flow conditions, to include the upper airway, more generations, and establishing more accurate flow conditions such as the tidal breathing.

REFERENCES

CHANG, H.K. and EL MASRY, O.A., (1982), "A Model Study of Flow Dynamics in Human Central Airways. Part I: Axial Velocity Profiles." *Resp. Physiol.*, **49**, 75-95.

KIM, C.S. and FISHER, D.M., (1999), "Deposition Characteristics of Aerosol Particles in Sequentially Bifurcating Airway Models." *Aerosol Sci. Technol*, **31**, 198-220.

MORSI, S.A. and ALEXANDER, A.J., (1972), "An Investigation of Particle Trajectories in Two-Phase Flow Systems." *J. Fluid Mech.*, **55**, 193-208.

SCHLESINGER, R.B., GURMAN, J.L. and LIPPMANN, M., (1982), "Particle deposition within bronchial airways: Comparisons using Constant and Cyclic Inspiratory Flows." *Ann Occup. Hyg.*, **26**, 47-64.

WEIBEL, E.R., (1963), *Morphometry of the Human Lung*, New York, Academic Press.

WILCOX, D.C., (1998), *Turbulence Modelling for CFD*, La Cañada, California, DCW Industries, Inc.

ZHANG, Z., KLEINSTREUER, C. and KIM, C.S., (2002), "Gas-solid Two-Phase Flow in a Triple Bifurcation Lung Airway Model." *Int. J. Multiphas. Flow*, **28**, 1021-1046.

ZHANG, Y. and FINLAY, W.H. (2005), "Measurement of the Effect of Cartilaginous Rings on Particle Deposition in a Proximal Lung Bifurcation Model." *Aerosol Sci. Tech.,* **39**, 394-399.